Specific Surface Areas of Porous Cu Manufactured by Lost Carbonate Sintering: Measurements by Quantitative Stereology and Cyclic Voltammetry

K.K. Diao, Z. Xiao and Y.Y. Zhao*

School of Engineering, University of Liverpool, Liverpool L69 3GH, UK

Abstract

Open-cell porous metals have many applications due to high surface area to volume ratios. Porous metals manufactured by the space holder methods have distinctively different porous structure from commercial open-cell metal foams, but very little research has been conducted to characterise the surface area of this class of materials. This paper measured the geometric, electroactive and real surface areas of porous Cu samples manufactured by the Lost Carbonate Sintering process by quantitative stereology and cyclic voltammetry. A cyclic voltammetry (peak current) procedure has been developed and successfully applied to the measurement of electroactive surface areas of the porous Cu. For porous Cu samples with pore sizes 75-1500 μm and porosities 0.5-0.8, the volumetric and gravimetric specific geometric, electroactive and real surface areas are in the ranges of 15-90 cm^{-1} and 5-45 cm^2/g, 200-400 cm^{-1} and 40-130 cm^2/g, and 1000-2500 cm^{-1} and 400-800 cm^2/g, respectively, varying with pore size and porosity. The geometric, electroactive and real surface areas are found to result from the contributions from primary porosity, primary and secondary porosities, and surfaces of metal particles, respectively. The measurement methods adopted in this study can provide vital information of surface areas at different length scales, which is important for many applications.

Key words: Microporous materials, surface properties, electrochemical techniques, optical metallography, powder metallurgy

* **Corresponding author**: y.y.zhao@liv.ac.uk; 0044 151 7944697

1. Introduction

Porous metals have attracted considerable attention in both academia and industry in the last few decades, due to their unique mechanical, thermal, acoustic, electrical and chemical properties[1-3]. Open-cell porous metals in particular have many potential applications such as heat exchange[4,5], sound absorption[6], catalyst support[2] and porous electrode [2]. High surface area is often desirable for these functional applications. In electrochemical applications, for instance, the reaction surface area of electrode is the most important characteristic[7] because high surface area means high energy density and thus better performance. Porous metals are therefore gradually replacing metal mesh electrodes in some applications, such as alkaline fuel cells, because of lower mass-to-surface ratio and lower cost[8].

Surface area of the porous metal is very sensitive to the manufacturing method. For similar pore size of 600 μm and porosity of 0.95-0.99, the Incofoam Ni foam produced by CVD has a surface area of 292 cm^2/g [8], while the Mitsubishi Ni foam produced by the slurry foaming method has a surface area of 19710 cm^2/g [9] (both measured by BET). However, the information on the surface area of porous metals manufactured by different methods is very limited in the literature.

Very little research has been conducted to date to understand the characteristics of the internal surfaces of porous metals manufactured by the space holder methods, which are an important family of methods developed recently for manufacturing open cell porous metals. In powder metallurgy based space-holder methods [3,10], a metal powder is first mixed with a sacrificial powder (space holder), such as NaCl [11], K_2CO_3 [12] or urea [13], and then compacted into a preform, followed by sintering. The space holder material is removed before, during or after sintering by either dissolution or decomposition to create pores. The metal particles are bonded during sintering to form a metal network.

The porous metals produced by powder metallurgy based space-holder methods have distinctively different internal pore architecture from the commercially available open-cell metal foams, e.g., Incofoam by CVD and ERG foam by investment casting[3]. The latter have lattice-like structure with high porosities (0.8-0.95) and the metal struts usually have a smooth surface. In contrast, the porous metals manufactured by the space-holder methods have lower porosities (0.5-0.85) and have porous structures with bimodal pores and rough internal surfaces. The primary pores are open pores randomly distributed in the metal matrix

and interconnected through small windows. They are effectively negative replicas of the particles of the space holder material, so their shapes, sizes and quantity are well defined. There are numerous secondary pores in the metal matrix. They are the small interstices or voids between the metal particles resulting from partial sintering. Up to date, no quantitative information on the surface area of this type of porous metals has been reported in the literature.

Surface area of porous metals is generally characterised either by geometric area or by true area, which can be different by more than two orders in magnitude. The active or effective surface area for a particular application depends on the length scale at which the surface plays a role. It is often greater than the geometric area but lower than the true area. Taking porous electrodes as an example, real surface area is important for energy storage applications such as super capacitors, because it directly determines the amount of charge stored [14,15]. In applications involving electrochemical reactions, however, the electroactive surface area, i.e., the area that effectively transfers the charge to the species in solution, is the key parameter. It depends on how well the electrolyte accesses the pores and is also influenced by the magnitude of the diffusion or Nernst layer in the electrolyte and the surface roughness of the electrode [16,17]. Electroactive surface area of the electrodes determines the maximum power or current density that can be achieved and therefore has a significant effect on the performance of the electrochemical cell.

This paper measures the surface areas, at different length scales, of porous Cu samples manufactured by the Lost Carbonate Sintering (LCS) process [12,18], which is a representative powder metallurgy based space holder method. The quantitative stereology (QS) method is used to determine the geometric surface area, i.e., surface area of the primary pores. Two cyclic voltammetry (CV) methods are used to measure the electroactive and real surface areas, which include contributions from both primary and secondary pores. Both volumetric and gravimetric surface areas are presented to facilitate comparisons with other porous metals on the basis of unit volume or unit mass. The effects of pore size and porosity on the surface areas are analysed. This study will provide a basis for quantitative understanding of the surfaces of porous metals produced by all solid route space holder methods. It also introduces the CV techniques to the measurements of effective surface areas of porous metals.

2. Experimental

2.1 Preparation of porous Cu samples

Porous Cu samples with different porosities and pore sizes were fabricated by the LCS process developed by Zhao and his colleagues [12,18]. The raw materials used in the experimental work were commercially pure Cu powder (Ecka Granules Metal Powder Ltd, UK) with a mean particle size of 72 μm (measured by Malvern Mastersizer 2000) and food grade K_2CO_3 powder (E&E Ltd, Australia) sieved into five different particle size ranges: 75-150 μm, 250-425 μm, 425-710 μm, 710-1000 μm and 1000-1500 μm. Each of these K_2CO_3 powders were mixed with the Cu powder at a pre-specified volume ratio according to the target porosity and then compacted into a preform under a pressure of 200 MPa. In fabricating a sample for QS measurement, the preform was first sintered at 850 °C for 2 h. The partly sintered sample was cut and ground when the K_2CO_3 particles were still in the preform so that a flat surface was obtained and the pores at the surface were not enlarged, filled or smeared during preparation. The sample was further sintered at 950 °C for 2 h. In fabricating a sample for CV measurements, the preform was directly sintered at 950 °C for 2 h. At this sintering stage, the Cu particles in the preform were fully bonded and the K_2CO_3 particles were decomposed, resulting in an open-cell porous Cu sample with a fixed porosity in the range of 0.5-0.8 and one of the five pore size ranges corresponding to the five K_2CO_3 particle sizes.

Figure 1 shows the typical porous structure of the porous Cu samples, obtained by SEM (JSM-6610, Japan). The large pores (primary pores) are negative replicas of the K_2CO_3 particles and are largely spherical. They are all interconnected to form an open cell network. The cell walls are formed by the sintering of Cu particles and have a structure characteristic of sintered materials, i.e., metal particles connected by sintering necks and interspersed with micro-voids (secondary pores).

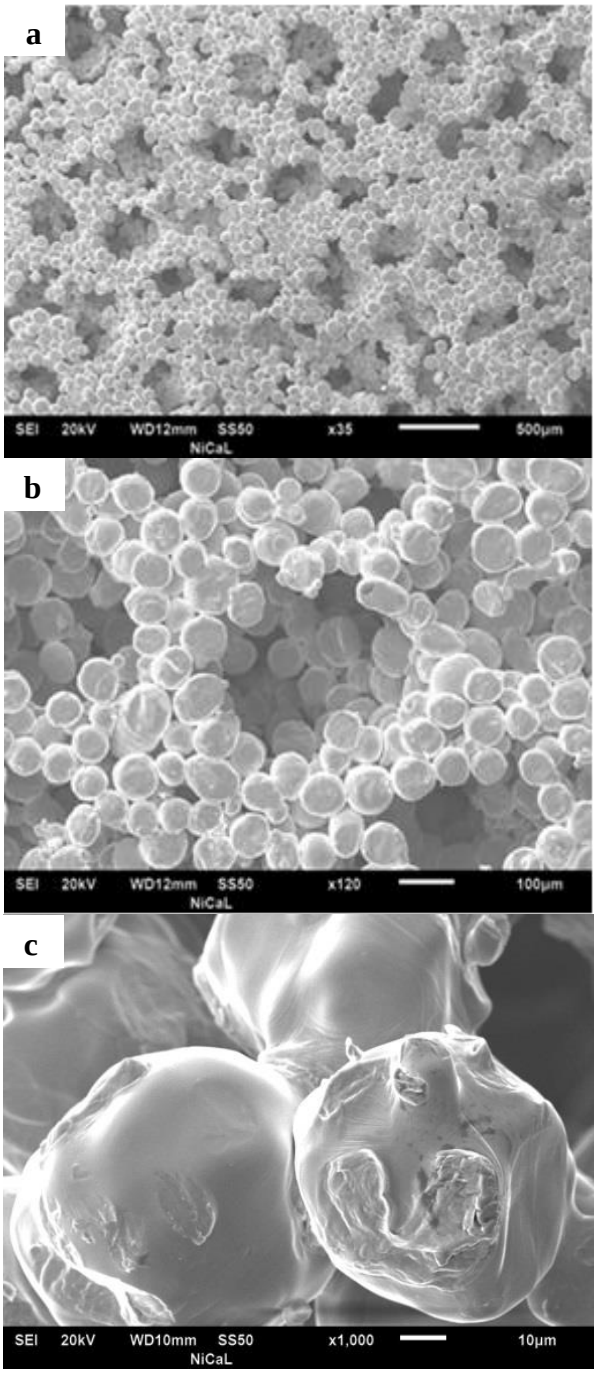

Figure 1: Microstructure of porous Cu (a) a global view, (b) morphology of pores and cell walls, and (c) sintering necks between Cu particles.

2.2 Measurement of geometric surface area by QS

QS was used to determine the geometric specific surface area of the porous Cu samples. Geometric surface area takes into account the total surface area of the primary pores formed by the K_2CO_3 particles, excluding the secondary pores (i.e., the interstices formed between

the Cu particles). The samples with the pore size of 75-150 µm were not measured by the QS method because of the difficulty in differentiating the primary and secondary pores.

An optical micrograph of the carefully-prepared flat surface of each porous cupper sample was taken by an optical microscope and a counting grid was superimposed onto the micrograph as shown in Figure 2. The Image-Pro Plus 6.0 software (Media Cybernetics Inc., USA) was used to identify and count the intercepts between the grid lines and the pore perimeters on the micrograph. The volumetric specific geometric surface area, S_{VG}, is the total internal surface area of the primary pores per unit volume of the sample and was obtained by [19]:

$$S_{VG} = \frac{2P}{L} \tag{1}$$

where P is the number of intercepts between the grid lines and the primary pore perimeters and L is the total length of the grid lines.

The gravimetric specific geometric surface area, S_{MG}, is the total internal surface area of the primary pores per unit mass of the sample and was calculated by:

$$S_{MG} = \frac{S_{VG}}{(1-\varepsilon)\rho} \tag{2}$$

where ε is the porosity of the sample and ρ is the density of solid Cu.

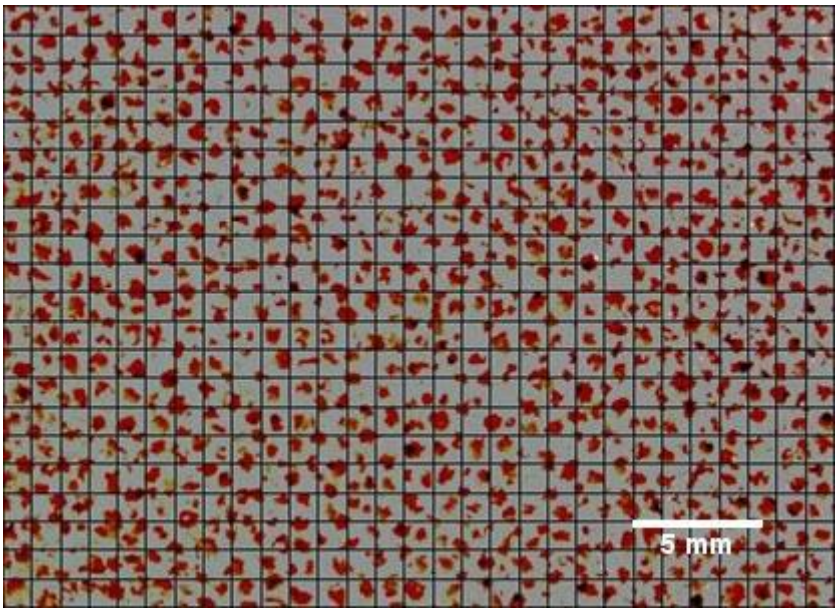

Figure 2: Optical micrograph of a porous Cu sample superimposed with a counting grid

2.3 Measurement of electroactive surface area by CV – peak current method

CV is a potentiodynamic electrochemical technique that can be used to analyse the redox reactions taking place at the surface of solid electrodes. For a redox reaction controlled by the diffusion of OH^-, the anodic or cathodic peak current in the cyclic voltammogram corresponding to the reaction can be expressed by Delahay equation [20]:

$$i_p = 3.67 \times 10^5 n^{\frac{3}{2}} A c D^{\frac{1}{2}} v^{\frac{1}{2}} \quad (3)$$

where i_p is the peak current, n is the number of electrons in the reaction, A is the surface area of the electrode, c is bulk concentration of OH^-, D is the diffusion coefficient of OH^- and v is the scan rate of the electrode potential.

Delahay equation cannot be used directly to calculate the surface area of Cu electrode due to passivation [20]. However, the peak current for a redox reaction is still proportional to the electrode surface area, although the proportionality coefficient may be different from that shown in equation (3).

In the current work, we propose a new approach to determine the electroactive surface area of a porous structure whose surface area is difficult to be measured by conventional methods. We first use a series of solid Cu plates with known surface areas to determine the proportionality coefficient of the Delahay relationship that is specifically applicable to Cu. We then use this relationship to determine the electroactive surface area of a porous metal electrode by measuring the peak current in the cyclic voltammogram.

Figure 3 shows a schematic diagram of the three-electrode electrochemical cell used for the CV measurements. The CV system consisted of a computerized potentiostat (Autolab PGSTAT101), working electrode (Cu plate or porous Cu sample), counter electrode (Pt plate for solid Cu samples and Pt coil for porous Cu samples), reference electrode (SCE) and electrolyte (0.1M KOH). The potential of the working electrode was varied between -1.55 and 0.8 V against the SCE reference electrode, with a scan rate of 0.026 V/s.

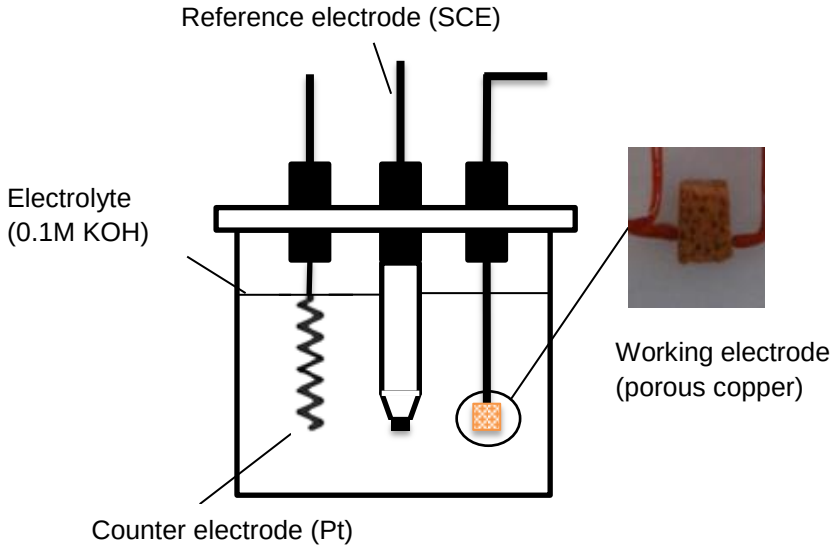

Figure 3: Schematic of the three-electrode electrochemical cell used for the CV measurements

A series of solid Cu plates with known geometric surface areas were used as working electrodes for calibration. Each Cu plate was first polished to 1 μm surface finish and then washed by 10% HCl, reducing the surface roughness to below 0.01 μm (measured by profiler PROSCAN 1000). The error of surface area caused by surface roughness was <0.01%. The Cu plate was fixed onto a nylon block with its edges sealed by resin and was connected to the potentiostat by a Cu wire.

A series of porous Cu samples were used as working electrodes for surface area measurement. Each porous Cu sample was cut to the dimensions of 0.3 cm × 0.4 cm × 0.5 cm, washed by 10% HCl and cleaned by ultrasonic treatment to ensure that complete infiltration of the sample by the electrolyte was achieved during the measurement. The porous Cu sample was connected to the potentiostat by two Cu wires coated with resin. The total surface area of the two contact points were less than 0.016 cm^2.

Figure 4a shows the cyclic voltammograms of three solid Cu plates with different known surface areas as examples. Three anodic peaks appeared in each voltammogram, corresponding to the following reactions [20].

$$2Cu + OH^- \rightarrow Cu_2O + H_2O + 2e \quad \text{(Peak I)} \quad \text{(4a)}$$

$$Cu_2O + 2OH^- + H_2O \rightarrow 2Cu(OH)_2 + 2e \quad \text{(Peak II)} \quad \text{(4b)}$$

$$Cu + 2OH^- \rightarrow CuO + H_2 + 2e \quad \text{(Peak III)} \quad \text{(4c)}$$

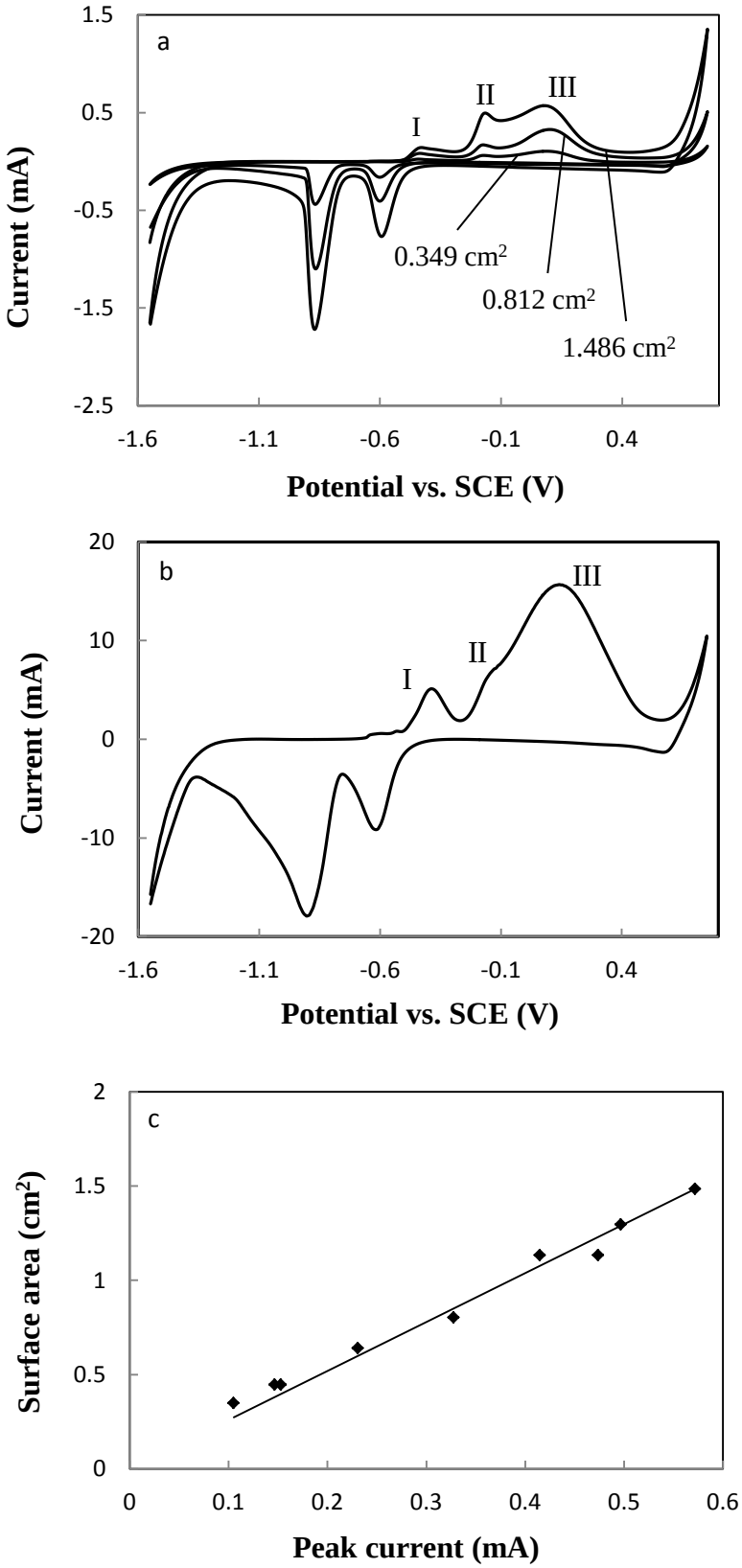

Figure 4: Cyclic voltammograms of (a) Cu plates with different surface areas and (b) a typical porous Cu sample. (c) Linear relation between Cu plate surface area and current of peak III.

In agreement with the CV tests carried out at slow scan rates [20], reaction (4c) is the predominant reaction, which is controlled by the diffusion of OH^- ions. Figure 4c shows that the peak current value of Peak III is directly proportional to the surface area of the Cu plate, so peak III was used in this work for the determination of surface area of porous Cu samples. The relationship between the electroactive surface area, A_E (cm^2), and peak current, I_p (mA), for the Cu plates is:

$$A_E = 2.60 \times I_p \quad (R^2 = 0.9791) \tag{5}$$

Figure 4b shows the voltammogram of a porous Cu sample. It is shown that it has the same shape as those of solid Cu both in the literature [20] and in the current tests (Figure 4a), indicating that the electrochemical processes at the surface of porous Cu are the same as those at the surface of solid Cu. The relation in Eqn. (5) should also be applicable to porous Cu.

The electroactive surface areas of the porous Cu samples were determined from Eqn. (5) by measuring the peak current values of Peak III under the same conditions as used for the solid Cu plates. The volumetric and gravimetric specific electroactive surface areas were obtained by dividing the electroactive surface area by the volume and mass of the sample, respectively.

2.4 Measurement of real surface area by CV – double layer capacitance method

The electrical double layer is a structure that describes the variation of electric potential near the electrode surface. The thickness of the double layer is usually thinner than 10 nm when the concentration of electrolyte is higher than 0.001 M [7]. A large amount of electrical charge can be stored in this very thin layer and the double layer capacitance depends on the electrode surface area. Therefore, measurement of double layer capacitance can be used to estimate the real surface area of solid metal electrodes [15,21].

The voltammograms of the solid and porous Cu working electrodes in the alkaline solution (Figures 4a and 4b) showed that the current was low and changed very little in the forward scan in the potential range from -1 to -0.75 V, indicating that there was no redox reactions and no Faradaic current in this potential range. This potential range was therefore chosen for the double layer capacitance measurements.

The double layer capacitance of each porous Cu sample was measured in the same three-electrode electrochemical cell shown in Figure 3. Figure 5a shows the cyclic voltammograms of a porous Cu sample in the non-Faradaic region with different scan rates. The double layer capacitance, C (mF), can be determined by [15]:

$$C = \frac{\Delta I}{v} \tag{6}$$

where ΔI (mA) is the change in current in the charge/discharge cycle and v (V/s) is the scan rate. The change in current was obtained by measuring the difference between the upper and bottom lines in the voltammogrm, as shown schematically in Figure 5a. In order to minimise measurement errors, a series of voltammograms were obtained at different scan rates and the change in current was plotted against scan rate, as shown in Figure 5b. The double layer capacitance of the sample is the proportionality coefficient between change in current and scan rate and was obtained by fitting the data to a straight line going through the origin.

Lukomska and Sobkowski [22] showed that the specific capacitance of the Cu/electrolyte interface is approximately 0.02 mF/cm^2, so the real surface area of porous Cu electrode, A_R (cm^2), can be estimated by:

$$A_R = \frac{C}{0.02} \tag{7}$$

The volumetric and gravimetric specific real surface areas can be obtained by dividing the real surface area by the volume and mass of the sample, respectively.

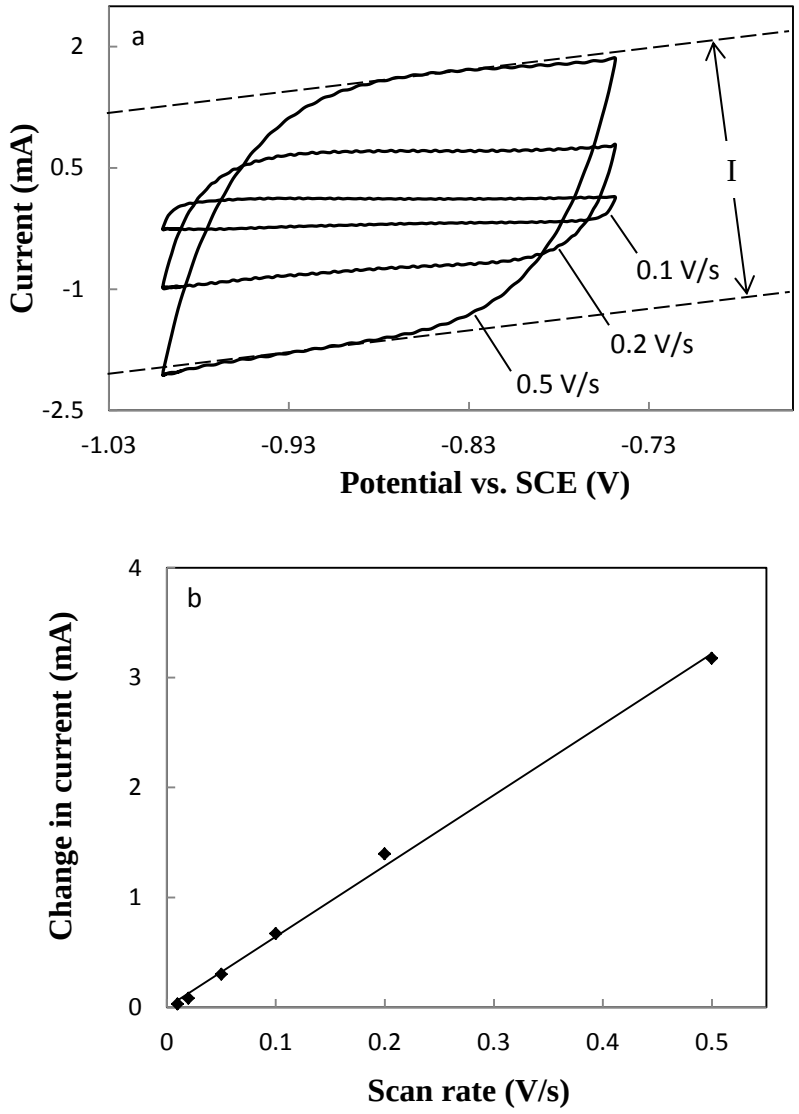

Figure 5: (a) Voltammograms of a porous Cu sample in the non-Faradaic region with different scan rates; (b) Linear relation between change in current and scan rate

3. Results

3.1 Geometric surface area

The variations of volumetric and gravimetric specific geometric surface areas, measured by the QS method described in 2.2, as a function of porosity and pore size are shown in Figure 6. In the porosity range 0.5-0.8 and pore size range 250-1500 μm, the volumetric and gravimetric specific geometric surface areas are in the ranges of 15-90 cm^{-1} and 5-45 cm^2/g, respectively. Both volumetric and gravimetric specific geometric surface areas increase with

porosity and decrease with pore size. However, volumetric specific geometric surface area is less sensitive to porosity.

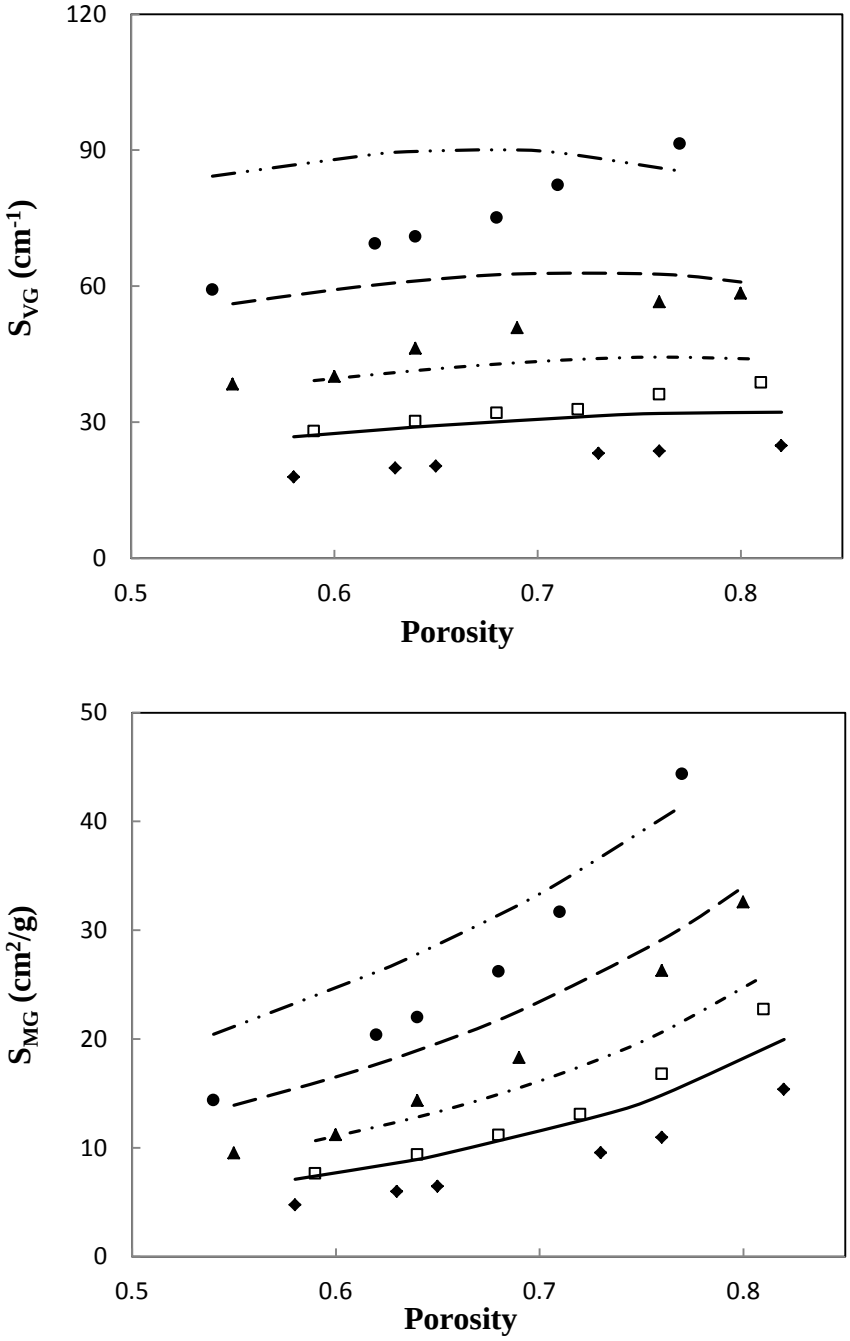

Figure 6: Variations of (a) volumetric (S_{VG}) and (b) gravimetric (S_{MG}) specific geometric surface areas with porosity at different pore sizes: experimental (● 250-425 µm, ▲ 425-710 µm, ▫ 710-1000 µm, ◆ 1000-1500 µm); modelling (–·–· 250-425 µm, – – – 425-710 µm, -·-·- 710-1000 µm, —— 1000-1500 µm)

3.2 Electroactive surface area

The variations of volumetric and gravimetric specific electroactive surface areas, measured by the CV – peak current method as described in 2.3, as a function of porosity and pore size are shown in Figure 7. In the porosity range 0.5-0.8 and pore size range 75-1500 μm, the volumetric and gravimetric specific electroactive surface areas are in the ranges of 200-400 cm^{-1} and 40-130 cm^2/g, respectively. The specific electroactive surface area is nearly one order of magnitude higher than the geometric surface area. The trends of the effects of porosity and pore size on electroactive surface area are less clear than those on the geometric surface area. In general, both volumetric and gravimetric specific electroactive surface areas decrease with pore size; the gravimetric specific electroactive surface area increases with porosity; the effect of porosity on the volumetric specific electroactive surface area is not pronounced.

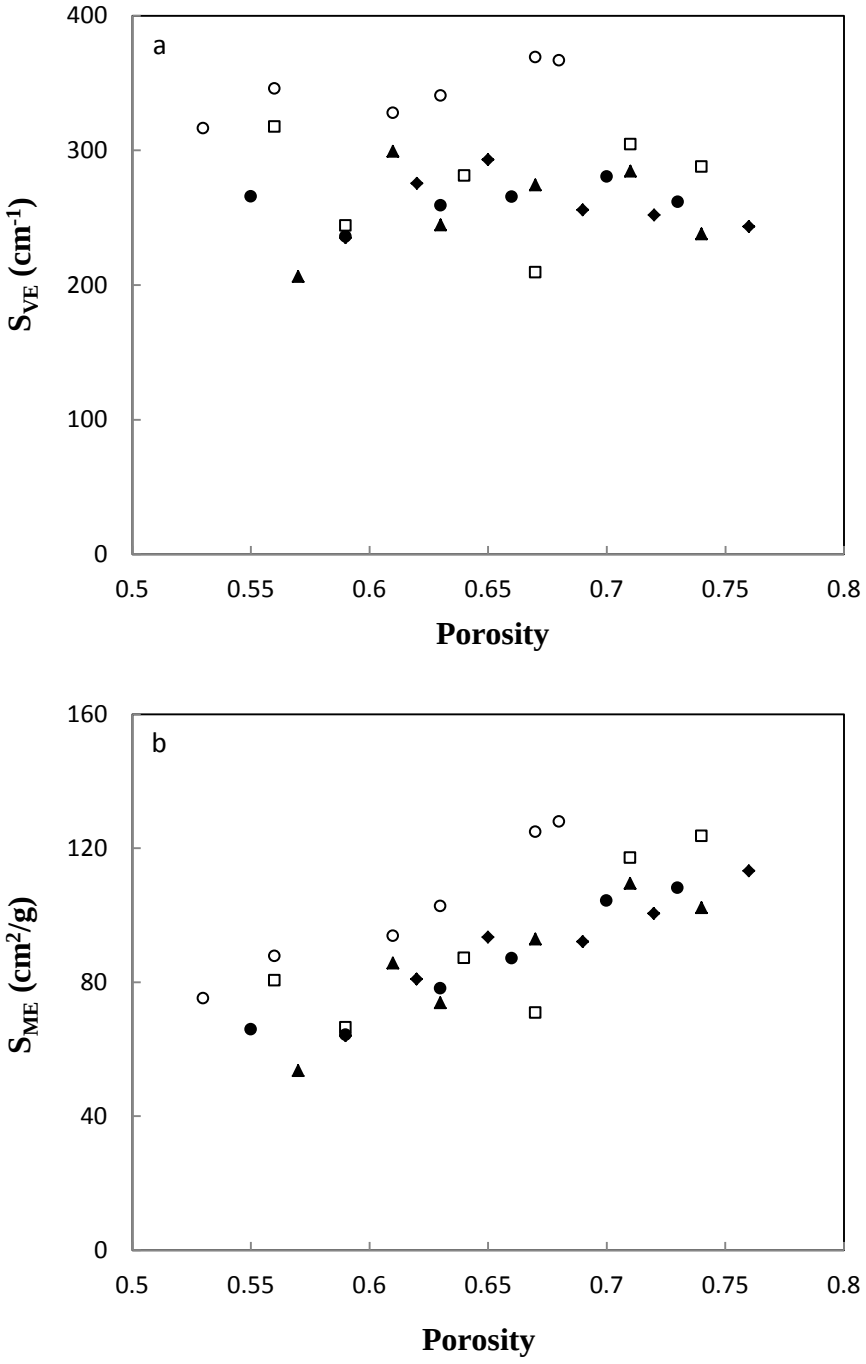

Figure 7: Variations of (a) volumetric (S_{VE}) and (b) gravimetric (S_{ME}) specific electroactive surface areas with porosity at different pore sizes: ○ 75-150 µm, ● 250-425 µm, ▲ 425-710 µm, □ 710-1000 µm, ◆ 1000-1500 µm

3.3 Real surface area

The variations of volumetric and gravimetric specific real surface areas, measured by the CV – double layer capacitance method as described in 2.4, as a function of porosity and pore size are shown in Figure 8. In the porosity range 0.5-0.8 and pore size range 75-1500 µm, the

volumetric and gravimetric specific real surface areas are in the ranges of 1000-2500 cm^{-1} and 400-800 cm^2/g, respectively. The specific real surface area is about one and two orders of magnitude higher than the electroactive and geometric surface areas, respectively. The trends of the effects of porosity and pore size on real surface area are again less clear than those on the geometric surface area. In general, the volumetric specific real surface area decreases with porosity while the gravimetric specific real surface area increases with porosity. The effect of pore size on the specific real surface areas is not pronounced.

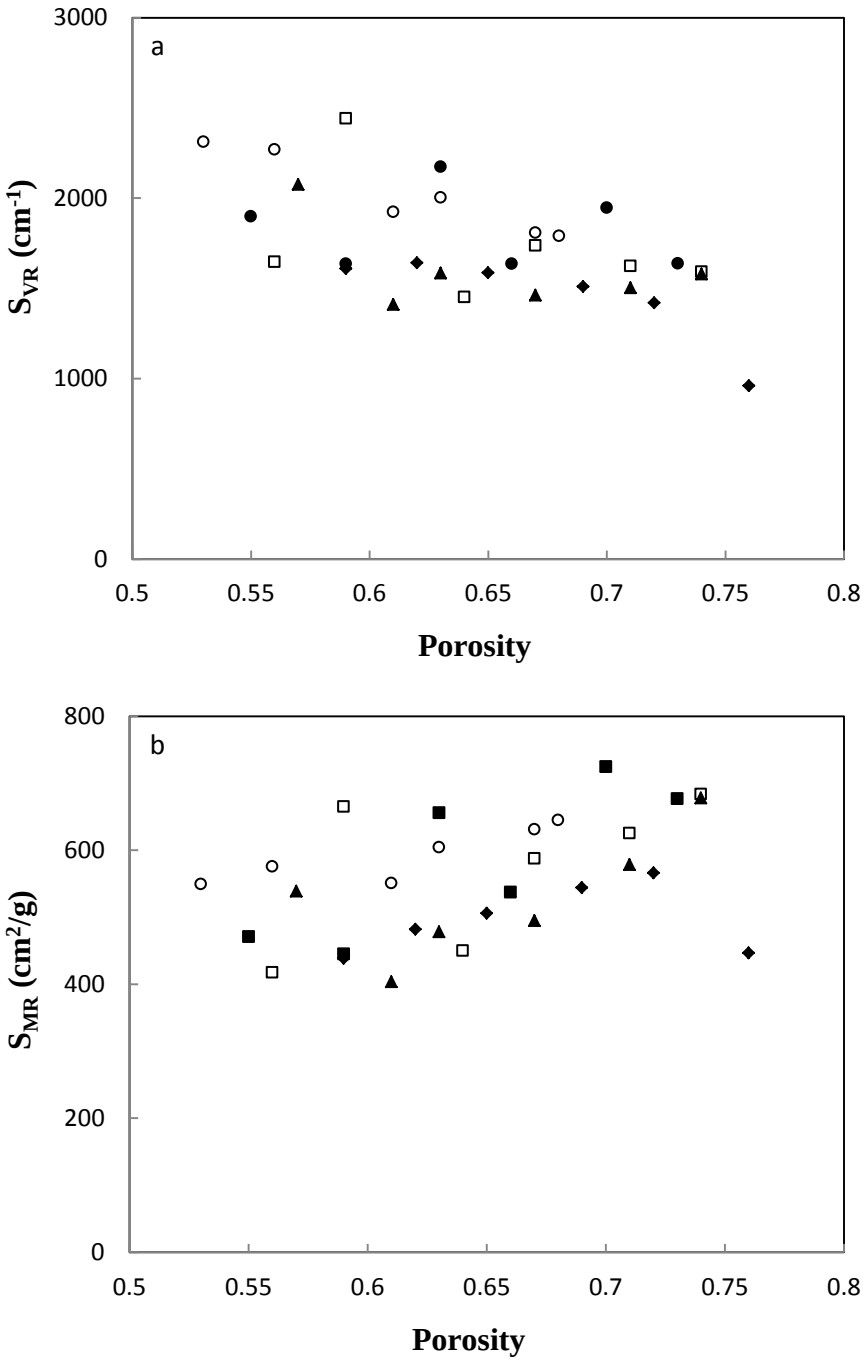

Figure 8: Variations of (a) volumetric (S_{VR}) and (b) gravimetric (S_{MR}) specific real surface areas with porosity at different pore sizes: ○ 75-150 µm, ● 250-425 µm, ▲ 425-710 µm, □ 710-1000 µm, ◆ 1000-1500 µm

4. Discussion

4.1 Geometric surface area

Geometry surface area is the total surface area of the cell walls of the primary pores in the porous sample. Because primary pores are in effect negative replicas of the K_2CO_3 particles used in the fabrication process, geometric surface area can be approximated by the total surface area of the K_2CO_3 particles less the area of the necks formed between the adjacent K_2CO_3 particles.

Zhao [23] analysed the connectivity of the NaCl particle network in an Al/NaCl compact used for manufacturing porous aluminium by the SDP process. Although the analysis was developed using SDP as an example, it is applicable to all powder metallurgy based space-holder methods, because these methods use the same principle to generate the porous structure. The analysis can be applied directly to LCS by substituting K_2CO_3 for NaCl and Cu for Al.

The direct contact between two spherical K_2CO_3 particles in the Cu/K_2CO_3 preform will form a neck, which will result in a window between the two resultant primary pores in the porous Cu sample. The magnitude of the neck depends on the relative sizes of the K_2CO_3 and Cu particles. The area of the sphere crown on the K_2CO_3 particle corresponding to the neck, A_c, can be calculated by [23]:

$$A_c = \frac{\pi}{2} d_p^2 \left(1 - \frac{\emptyset+2}{\sqrt{\emptyset^2+6\emptyset+5}}\right) \quad (8)$$

where d_p is the diameter of the K_2CO_3 particle (effectively, the pore size) and $\emptyset$ is the K_2CO_3-to-Cu particle size ratio, i.e., the ratio between the diameters of the K_2CO_3 and Cu particles, d_p and d_{Cu}, respectively.

The average number of K_2CO_3/K_2CO_3 contacts on a single K_2CO_3 particle in the Cu/K_2CO_3 powder mixture, μ, depends not only on the K_2CO_3-to-Cu particle size ratio, $\emptyset$, but also on the volume fraction of the K_2CO_3 in the mixture (which is effectively the porosity of the resultant porous Cu, ε) and can be calculated by [23]:

$$\mu = \frac{2}{\left(1-\frac{\emptyset+2}{\sqrt{\emptyset^2+6\emptyset+5}}\right)\left(1-\emptyset+\frac{\emptyset}{\varepsilon}\right)} \quad (9)$$

The surface area of each pore is therefore the surface area of the K_2CO_3 particle less the total area of the sphere crowns forming the necks. The volumetric specific geometric surface area of the porous Cu, i.e., the total surface area of the primary pores per unit volume, can thus be calculated by:

$$S_{VG} = \frac{A_p - \mu A_c}{V_p/\varepsilon} = \frac{6}{1/\varepsilon + 1/[(1-\varepsilon)\emptyset]} = \frac{6}{d_p/\varepsilon + d_{Cu}/(1-\varepsilon)} \quad (10)$$

where A_p and V_p are the surface area and volume of a K_2CO_3 particle, respectively. The gravimetric specific geometric surface area can be calculated accordingly by:

$$S_{MG} = \frac{S_{VG}}{(1-\varepsilon)\rho} = \frac{6}{\rho[d_{Cu} + d_p(1-\varepsilon)/\varepsilon]} \quad (11)$$

Eqs. (10) and (11) show that the volumetric specific surface area of LCS porous Cu is a function of porosity, ε, K_2CO_3 particle size or pore size, d_p, and Cu particle size, d_{Cu}. The gravimetric specific surface area is also a function of the density of Cu, ρ. Although the particles of the K_2CO_3 and Cu powders used in this experiment have a size range instead of a uniform size, it is possible to estimate the volumetric and gravimetric specific surface areas using mean particle sizes.

The calculated values of the volumetric and gravimetric surface areas for the porous Cu samples are shown in Figure 6 alongside the experimental values. The calculations were carried out using Eqs. (10) and (11) with the following input values: density of Cu ρ = 8.9 g/cm^3, mean Cu particle diameter d_{Cu} = 72 µm, and mean K_2CO_3 particle diameters d_p = 338 µm, 568 µm, 855 µm and 1250 µm for the particle size ranges 250-425 µm, 425-710 µm, 710-1000 µm and 1000-1500 µm, respectively. Figure 6 shows that the experimental values generally follow the trends predicted by this model, indicating that the model gives a reasonable quantitative description of the major controlling factors for surface area. However, the calculated values are higher than the measured results. This is likely due to the approximations of the broad particle size ranges of the K_2CO_3 and Cu powders by single particle sizes.

The volumetric and gravimetric specific geometric surface areas of the LCS porous Cu are in the ranges of 15-90 cm^{-1} and 5-45 cm^2/g, which are in the same orders of magnitude as those of Incofoam Ni foam (20 cm^2/g [24]) and those of VITO foam (14.1 cm^{-1} for stainless steel and 42.5 cm^{-1} for Ti foam, both determined by micro-CT [25]).

4.2 Electroactive surface area

Figure 9 shows the ratio of electroactive and geometric surface areas (same for volumetric and gravimetric) as a function of mean pore size at different porosities. Because the samples used for QS and CV measurements had slightly different porosities, the ratio values could not be obtained directly from the experimental data. For each sample with a measured volumetric specific electroactive surface area shown in Figure 7(a), the volumetric specific geometric surface area was obtained by interpolation of the data in Figure 6(a) based on the porosity of the sample. The ratio was simply the former divided by the latter. The volumetric specific geometric surface areas of the samples with the smallest pore size range 75-150 μm were calculated using Eq. (10), because no experimental data were available.

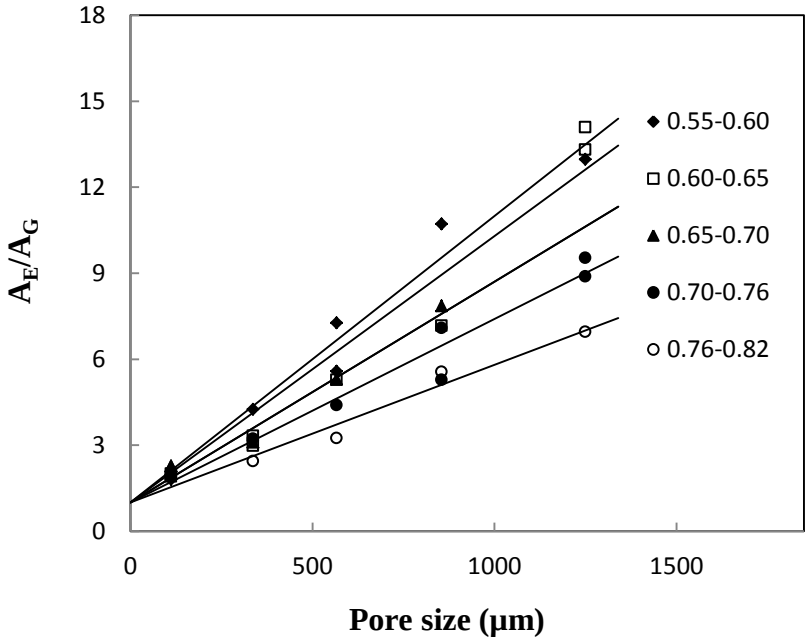

Figure 9: Variation of the ratio between the electroactive (A_E) and geometric (A_G) surface areas with mean pore size at different porosities

Figure 9 shows that the ratio of electroactive and geometric surface areas increases nearly linearly with mean pore size and generally increases with decreasing porosity. An especially interesting characteristic of the trendlines is that their intercepts at the vertical axis are all unity, indicating that there are more surfaces contributing to the electrochemical reactions and peak current than the geometric surface area. The electroactive surface area can be separated into two parts: contribution from the primary porosity (geometric surface area) and contribution from the secondary porosity, i.e., the voids or interstices inside the Cu matrix.

The contribution to the electroactive surface area from the secondary porosity can be significantly greater than the geometric surface area (up to 14 times as shown in Figure 9). This high contribution is due to the numerous small voids or interstices in the Cu matrix as a consequence of incomplete densification of Cu particles during sintering. The network formed by these voids, i.e., the secondary porosity, can be penetrated by the electrolyte and therefore make significant contributions to the electroactive surface area.

It can be seen from Figure 9 that the contribution to the electroactive surface area from the secondary porosity is proportional to pore size and decreases with porosity. The effect of porosity on the ratio between electroactive and geometric surface areas can be explained by the relative quantities of Cu particles in the interior and exterior regions in the solid matrix. For a fixed pore size, increasing porosity means more Cu particles are located in the surface region and the number of Cu particles residing in the interior region is reduced. Relative to the contribution of the primary porosity to the electroactive surface area (i.e., geometric surface area), the contribution of the second porosity decreases. Therefore, the ratio between electroactive and geometric surface areas decreases with porosity. The effect of pore size is likely a manifestation of the effect of the diffusion layer on the concentration distribution of the electroactive species.

The diffusion layer thickness for the diffusion of OH^- towards Cu electrode can be calculated by [26]:

$$\sigma = \sqrt{\frac{DRT}{nFv}} \tag{12}$$

where D ($2\times10^{-5}cm^2/s$) is the diffusion coefficient of OH^-, R is the gas constant (8.134 J/K mol), T is the temperature (298K), n is the number of electronic transfer (2 for reaction 4c), F is the Faraday constant (96485 C/mol) and v is the scan rate (0.026 V/s in this work). Under the current experimental conditions, the diffusion layer thickness for a flat surface is calculated to be about 31 μm. This is about 1/2 to 1/20 of the pore radius. The actual thickness of the region with low concentrations of electroactive species is even greater and occupies a significant portion of the pores.

For small pores with a radius comparable to the diffusion layer thickness, a large proportion of the electrolyte is within the diffusion layer. Only a small reservoir of electrolyte in the central region of the pore has the initial concentration of the electroactive species. The

electroactive species in the electrolyte is consumed rapidly during the CV measurement. In addition, acute curvature associated with small pores also leads to a greater actual diffusion layer than that predicted for a flat surface. All these factors reduce the concentrations of the electroactive species in the region next to the electrode surface, leadings to a reduced peak current and thus a reduced electroactive surface area.

With increasing pore sizes, the reservoir of electrolyte with the initial concentration of the electroactive species becomes bigger. The diffusion layer thickness also approaches that predicted for a flat surface due to reduced curvature. As a consequence, the region of depleted electroactive species next to the pore walls is reduced, leadings to an increased peak current and thus an increased electroactive surface area.

4.3 Real surface area

The real surface area measured by the double layer capacitance method accounts for all surfaces in the porous Cu sample which can be reached by the electrolyte. Because of insufficient densification of Cu particles during sintering in LCS, the majority of the voids or interstices between the Cu particles are interconnected and therefore contribute to the real surface area. The real surface area is therefore the total surface area of all Cu particles, excluding the sintering necks between the Cu particles and the small number of isolated voids.

Figure 10 plots the volumetric specific real surface area (S_{VR}) versus the theoretical volumetric specific surface area of the Cu particles (S_{VCu}), which is defined as the total surface area of all Cu particles per unit volume of the porous sample and is calculated by assuming that all Cu particles are perfect spheres of 72 μm diameter with a smooth surface. It shows that there is a strong correlation between the real surface area of the porous Cu sample and the total surface area of the Cu particles in the sample. The former is about 5.8 times of the latter. This difference can be accounted for by the surface roughness of the Cu particles. As shown in Figure 1c, the particles of the Cu powder used in this work are neither spherical nor smooth surfaced. The actual surface area of a Cu particle is much higher than predicted by assuming a perfect sphere.

The volumetric and gravimetric specific real surface areas of the LCS porous Cu are in the ranges of 1000-2500 cm^{-1} and 400-800 cm^2/g, which are higher than those of the Incofoam Ni foam (292 cm^2/g, measure dby BET [8]) but considerably lower that those of the Mitsubishi Ni foam (19710 cm^2/g, measured by BET [9]).

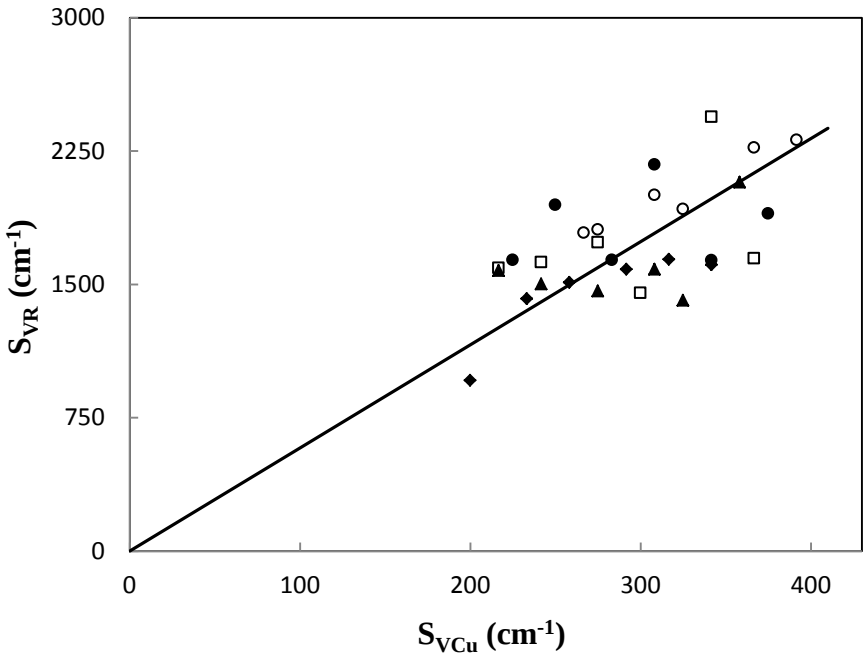

Figure 10: Volumetric specific real surface area of porous Cu sample (S_{VR}) versus the theoretical volumetric specific surface area of the Cu particles (S_{VCu}) for different pore sizes: ○ 75-150 µm, ● 250-425 µm, ▲ 425-710 µm, □ 710-1000 µm, ◆ 1000-1500µm.

5. Conclusions

1) A cyclic voltammetry (peak current) procedure has been developed to measure electroactive surface area of porous metals.
2) Geometric, electroactive and real surface areas of porous Cu samples manufactured by the LCS process, with pore sizes 75-1500 μm and porosities 0.5-0.8, have been measured successfully by quantitative stereology, cyclic voltammetry (peak current) and cyclic voltammetry (double layer capacitance) methods, respectively.
3) The volumetric and gravimetric specific geometric surface areas are in the ranges of 15-90 cm^{-1} and 5-45 cm^2/g, respectively. They increase with porosity and decrease with pore size. Geometry surface area is due to the contribution from primary porosity only. It is a function of porosity, pore size and Cu particle size, and can be described by the analytical model in Ref [24].
4) The volumetric and gravimetric specific electroactive surface areas are in the ranges of 200-400 cm^{-1} and 40-130 cm^2/g, respectively. Electroactive surface area consists of contributions from primary and secondary porosities. The latter contribution increases with pore size and decreases with porosity.
5) The volumetric and gravimetric specific real surface areas are in the ranges of 1000-2500 cm^{-1} and 400-800 cm^2/g, respectively. Real surface area is the total surface area of all Cu particles less the sintering necks and isolated voids, and has a strong correlation with the total geometric surface area of all the Cu particles in the sample.

References

[1] Gibson L.J., Ashby M.F., Cellular Solids: Structure and Properties, 2nd ed., Cambridge University Press, Cambridge, 1999.

[2] Ashby M.F., Metal Foams: A Design Guide, Butterworth-Heinemann, Boston, 2000.

[3] Banhart J., Manufacture, Characterisation and Application of Cellular Metals and Metal Foams, Progress in Materials Science 46 (2001) 559.

[4] Zhang L.P., Mullen D., Lynn K., Zhao Y.Y., Heat Transfer Performance of Porous Copper Fabricated by the Lost Carbonate Sintering Process, Materials Research Society Symposium Proceedings, 1188 (2009) 07.

[5] Xiao Z., Zhao Y.Y., Heat Transfer Coefficient of Porous Copper with Homogeneous and Hydrid Structures in Active Cooling, Journal of Materials Research 28 (2013) 2545.

[6] Han F., Seiffert G., Zhao Y.Y., Gibbs B., Acoustic Absorption Behaviour of an Open-Celled Aluminium Foam, Journal of Physics D: Applied Physics 36 (2003) 294-302.

[7] Scholz F., Electroanalytical Methods: Guide to Experiments and Applications, Springer, Berin, 2002.

[8] Bidault F., Brett D.J.L., Middlenton P.H., A New Application for Nickel Foam in Alkaline Fuel Cells, International Journal of Hydrogen Energy 34 (2009) 6799.

[9] Dukic A., Alar V., Firak M., Jakovljevic S., A significant improvement in material of foam, Journal of Alloys and Compounds 573(2013) 128-132.

[10] Zhao Y.Y., Porous Metallic Materials Produced by P/M Methods, Journal of Powder Metallurgy & Mining 2 (2013) e113.

[11] Zhao Y.Y., Sun D.X., A Novel Sintering-Dissolution Process for Manufacturing Al Foams, Scripta Materialia 44 (2001) 105.

[12] Zhao Y.Y., Fung T., Zhang L.P., Lost Carbonate Sintering Process for Manufacturing Metal Foams, Scripta Materialia 52 (2005) 295.

[13] Laptev A., Bram M., Buchkremer H.P., Stover D., Study of Production Route for Titanium Parts Combining very High Porosity and Complex Shape, Powder Metallurgy 47 (2004) 85-92.

[14] Li Y., Chang S., Liu X., Nanaostructured CuO Directly Grown on Copper Foam and Their Supercapacitance Performance, Electrochimica Acta 85 (2012) 393.

[15] Lewandowski A., Jakobczyk P., Galinski M., Capacitance of Electrochemical Double Layer Capacitors, Electochimica Acta 86 (2012) 225.

[16] Davies T.J., Banks C.E., Compton R.G., Voltammetry at Spatially Heterogeneous Electrodes, Journal of Solid State Electrochemistry, 9 (2005) 797.

[17] Ward K.R., Gara M., Lawrence N.S., The Effective Electrochemical Rate Constant for Non-flat and Non-uniform Electrode Surfaces, Journal of Electroanalytical Chemistry 695 (2013) 1.

[18] Zhang .P., Zhao Y.Y., Fabrication of High Melting-Point Porous Metals by Lost Carbonate Sintering Process via Decomposition Route, Journal of Engineering Manufacture 222 (2008)267.

[19] Underwood E., Quantitative stereology, Addison-Wesley, Reading, 1970.

[20] Ambrose J., Barradas R.G., Shoesmith D.W., Investigations of Copper in Aqueous Alkaline Solutions by Cyclic Voltammetry, Journal of Electroanalytical Chemistry and Interfacial Electrochemistry 47 (1973) 47.

[21] Brevnov D.A., Olson T.S., Double-Layer Capacitors Composed of Interconnected Silver Particles and with a High-Frequency Response, Electrochimica Acta 51 (2006) 1172.

[22] Lukomska A., Sobkowski J., Potential of Zero Charge of Monocrystalline Copper Electrodes in Perchlorate Solutions, Journal of Electroanalytical Chemistry 567 (2004) 95-102.

[23] Zhao Y.Y., Stochastic Modelling of Removability of NaCl in Sintering and Dissolution Process to Produce Al Foams, Journal of Porous Materials 10 (2003) 105-111.

[24] Tseng C., Tsai B., Liu Z., Cheng T., Chang W., Lo S., A PEM fuel cell with metal foam as flow distributor, Energy Conversion and Management 62 (2012) 14-21.

[25] Van Cleynenbreugel T., Schrooten J., Van Oosterwyck H., Vander Sloten J., Micro-CT-based screening of biomechanical and structural properties of bone tissue engineering scaffolds, Medical & Biological Engineering & Computing 44 (2006) 517–525.

[26] Prasad M.A., Sangaranarayanan M.V., Formulation of a Simple Analytical Expression for Irreversible Electron Transfer Processes in Linear Sweep Voltammetry and Its Experimental Verification, Electrochimica Acta 49 (2004) 2569-2579.